Imaging and Control of Magnetic Domains in a Quasi-One-Dimensional Quantum Antiferromagnet $BaCu_2Si_2O_7$

Masato Moromizato,[1] Takeshi Miyake,[2] Takatsugu Masuda,[2] Tsuyoshi Kimura,[3] and Kenta Kimura[4,*]
[1]Department of Advanced Materials Science, University of Tokyo, Chiba 277-8561, Japan
[2]Institute for Solid State Physics, The University of Tokyo, Chiba 277-8581, Japan
[3]Department of Applied Physics, The University of Tokyo, Tokyo 113-8656, Japan
[4]Department of Materials Science, Osaka Metropolitan University, Osaka 599-8531, Japan

(Received 6 January 2024; revised 15 June 2024; accepted 12 July 2024; published 22 August 2024)

We visualize antiferromagnetic domains in a representative quasi-one-dimensional $S = 1/2$ quantum antiferromagnet, $BaCu_2Si_2O_7$, using nonreciprocal directional dichroism, which differentiates the optical absorption of a pair of antiferromagnetic domains. Opposite antiferromagnetic domains, each about submillimeter in size, are found to coexist in a single-crystal specimen, and the domain walls run predominantly along the spin chains. We also demonstrate that the domain walls can be moved by an applied electric field through a magnetoelectric coupling and that the direction of the domain walls is maintained during the motion. We explain the domain wall anisotropy by the quasi-one-dimensional nature of the exchange interactions. This Letter will contribute to the understanding of the domain physics of quasi-one-dimensional quantum antiferromagnets.

DOI: 10.1103/PhysRevLett.133.086701

Quasi-one-dimensional quantum antiferromagnets (q1D-QAFMs) consist of chains (or ladders) of magnetic ions with a small spin quantum number such as $S = 1/2$ and 1, where intrachain interactions are much stronger than interchain interactions. Intensive studies over the last century have shown that the combination of strong quantum spin fluctuations and low dimensionality can lead to a variety of unconventional quantum phenomena [1,2]. For example, when the interchain coupling is sufficiently small, quantum mechanical states, such as a quantum spin liquid [3], a Haldane gap state [4,5], and a spin nematic phase [6], can form. In contrast, when the strength of the interchain coupling is non-negligible, long-range order (LRO) takes place. The properties of such an LRO for q1D-QAFMs differ from those of conventional three-dimensional (3D) AFMs, as manifested by a transition temperature T_N much lower than the energy scale of intrachain interactions, extremely reduced ordered magnetic moments, and unconventional excitations [7–14]. As in 2D and 3D AFMs, the LRO in q1D-QAFMs will form a pair of domain states with opposite directions of magnetic moments (see Fig. 1). Domains in 2D and 3D AFMs have recently been intensively studied with respect to their spintronic applications [15,16]. For q1D-QAFMs, it has been discussed that domain walls (DWs) separating opposite domains dominate the thermodynamic properties [17–19]. However, the observation of domain patterns in q1D-QAFMs seems to be challenging because the reduced ordered moments result in vanishingly small stray fields from the sample surfaces and domain boundaries, making the use of neutron topography [20] and magnetic force microscopy [21] difficult. In addition, the low T_N does not favor an intense laser that can heat up a sample above T_N, making the use of nonlinear optics difficult [22]. In fact, there has been no experimental observation of the domain pattern in q1D-QAFMs.

Nonreciprocal directional dichroism (NDD) [23–27], i.e., a change in optical absorption by reversing the direction of light propagation or the sign of magnetic order parameters, has recently been shown to be an effective tool for visualizing antiferromagnetic (AF) domain patterns by differentiating the absorption between the opposite AF domains [28–31], as schematically illustrated in Fig. 1. The NDD is closely related to a linear magnetoelectric (ME) effect [32], which is an induction of electric polarization $\mathbf{P}$ (magnetization $\mathbf{M}$) by a magnetic field $\mathbf{H}$ (electric field $\mathbf{E}$) [26]. When electromagnetic waves (or light) with an angular frequency ω travel in a medium with off-diagonal elements of the linear ME tensor χ, the oscillating $\mathbf{P}^\omega$ is induced by the $\mathbf{H}^\omega$ of light ($\mathbf{P}^\omega_H$) and can interfere with the oscillating $\mathbf{P}^\omega$ induced by the $\mathbf{E}^\omega$ of light ($\mathbf{P}^\omega_E$). When the direction of light propagation or the sign of the AF order parameters is reversed, the sign of $\mathbf{P}^\omega_H$ is reversed with respect to that of $\mathbf{P}^\omega_E$. As a result, the constructive interference is transformed into the destructive interference, leading to NDD. Since both space-inversion and time-reversal symmetries must be broken for the linear ME effect to occur, the NDD must also satisfy the same symmetry requirements.

In this Letter, we use the NDD to visualize the AF domain pattern of the representative $S = 1/2$ q1D-QAFM,

*Contact author: kentakimura@omu.ac.jp

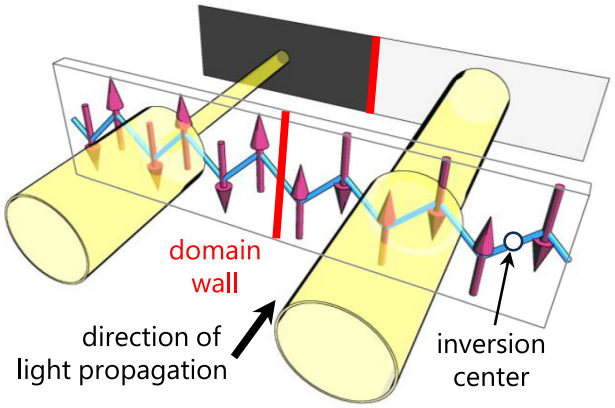

FIG. 1. Conceptual illustration of the visualization of the antiferromagnetic (AF) domains in a quasi-one-dimensional quantum antiferromagnet via the nonreciprocal directional dichroism (NDD). Yellow transparent cylinders denote light beams propagating along the direction of the thick black arrow. The diameter of the cylinders represents the intensity of the light beams. In the AF phase, the magnetic moments (magenta arrows) are in principle antiparallel. However, the parallel alignment of the magnetic moments can appear as a defect called a domain wall (red line). For certain lattice geometries, the AF phase breaks both time-reversal and space-inversion symmetries and thus allows the NDD, which differentiates the absorption of opposite domain states separated by the domain wall. Consequently, AF domains can be visualized as the difference in the intensity of light transmitted through a sample. A zigzag structure shown in this figure is an example of such a lattice geometry, where the AF order removes inversion centers at the midpoints of every two neighboring sites (represented by a circle), thus breaking both space-inversion and time-reversal symmetries.

$BaCu_2Si_2O_7$ [10], whose AF phase breaks both time-reversal and space-inversion symmetries, as described later. We observe anisotropic DWs running along the spin chains. We also observe a motion of the DWs driven by an applied electric field. The direction of the DWs is maintained during the motion. These results are an important step toward understanding the domain physics in q1D-QAFMs.

$BaCu_2Si_2O_7$ crystallizes in an orthorhombic crystal structure (space group $Pnma$), in which corner-sharing CuO_4 plaquettes form zigzag chains of $S = 1/2$ Cu^{2+} spins [10], as shown in Figs. 2(a) and 2(b). The intrachain interaction (J) between Cu^{2+} is antiferromagnetic ($|J| = 280$ K) and 2 orders of magnitude larger than the interchain interactions (J_x, J_y, and J_3), making $BaCu_2Si_2O_7$ as a model $S = 1/2$ q1D-QAFM [9,33]. The weak interchain interaction leads to the AF LRO at $T_N = 9.2$ K. The ordered magnetic moments in this AF phase are parallel to the c axis and are significantly reduced to as small as 0.1 μ_B/Cu by quantum fluctuations in the absence of external magnetic fields [9,33]. Figures 2(a) and 2(b) show the magnetic structures for a pair of AF domains with opposite magnetic moments. These domains are labeled as AF+ and AF−. Note that while the crystal structure is centrosymmetric, the Cu site is locally noncentrosymmetric due to the zigzag chain configuration. In addition, a pair of Cu ions related by the inversion center [marked with a white circle in Fig. 2(a)] have the opposite magnetic moments. Consequently, the magnetic structure breaks both space-inversion and time-reversal symmetries [34]. The magnetic point group is $m'mm$, which allows finite off-diagonal elements of the ME tensor, χ_{bc} and χ_{cb}, and correspondingly the NDD for the light propagation vector $\mathbf{k}$ along the a axis (k_a). However, neither the linear ME effect nor the NDD has been reported so far. Among a number of q1D-QAFMs with pronounced ME effect (e.g., $TlCuCl_3$ [35], Sul-Cu_2Cl_4 [36], and $LiCuVO_4$ [37]), $BaCu_2Si_2O_7$ is a rare instance with broken space-inversion and time-reversal symmetries at $H = 0$, making it suitable for imaging the domains of q1D-QAFMs without external fields.

Single crystals of $BaCu_2Si_2O_7$ were grown by the floating zone method [10]. The dielectric constant ε and $\mathbf{P}$ along the c axis (ε_c and P_c) in $\mathbf{H}$ along the b axis (H_b) were measured to investigate the linear ME effect, more specifically $P_c = \chi_{cb} H_b$. The applied H_b was limited to 6 T, which is well below a critical field for a spin-flop transition [38]. Optical absorption (α) spectra for k_a in the photon energy range $1.35 < E_{ph} < 2.80$ eV were measured using a home-built fiber-based optical system [29]. The incident light was linearly polarized along either the b ($\mathbf{E}^\omega \| b$) or c ($\mathbf{E}^\omega \| c$) axis. Domain imaging experiments were performed using a home-built horizontal polarized microscope in transmittance geometry [29]. The details of the experiments are described in the Supplemental Material [39]. The crystal structures in Fig. 2 were drawn by using VESTA software [40].

Figure 2(c) shows the temperature (T) dependence of ε_c. It exhibits a sharp peak at T_N at applied H_b, the magnitude of which is increased at higher H_b. Also, as shown in Fig. 2(d), a finite P_c is induced by H_b below T_N, and its magnitude increases linearly with H_b (compare P_c at 3 and 6 T). These results are fully consistent with the existence of the linear ME effect, thus confirming the breaking of time-reversal and space-inversion symmetries in the AF phase of $BaCu_2Si_2O_7$.

Figure 2(e) shows the α spectrum for $\mathbf{E}^\omega \| b$ at 4.2 K in the absence of external fields. Broad peaks are visible at about 1.6, 1.9, and 2.2 eV, which can be attributed to Cu^{2+} d-d transitions. It has recently been shown that the Cu^{2+} d-d transitions in copper-based oxides often give rise to large NDD signals [25,29]. To study the NDD in $BaCu_2Si_2O_7$, we measure the difference between α of the AF+ and AF− domains, i.e., $\Delta\alpha = \alpha(\mathrm{AF+}) - \alpha(\mathrm{AF-})$. Since the AF+ and AF− states have χ_{cb} of opposite sign, the simultaneous application of H_b and $\mathbf{E}$ along the c axis (E_c) can stabilize one state over the other through the ME coupling [32]. In the present experiment, the AF+ and AF− states were

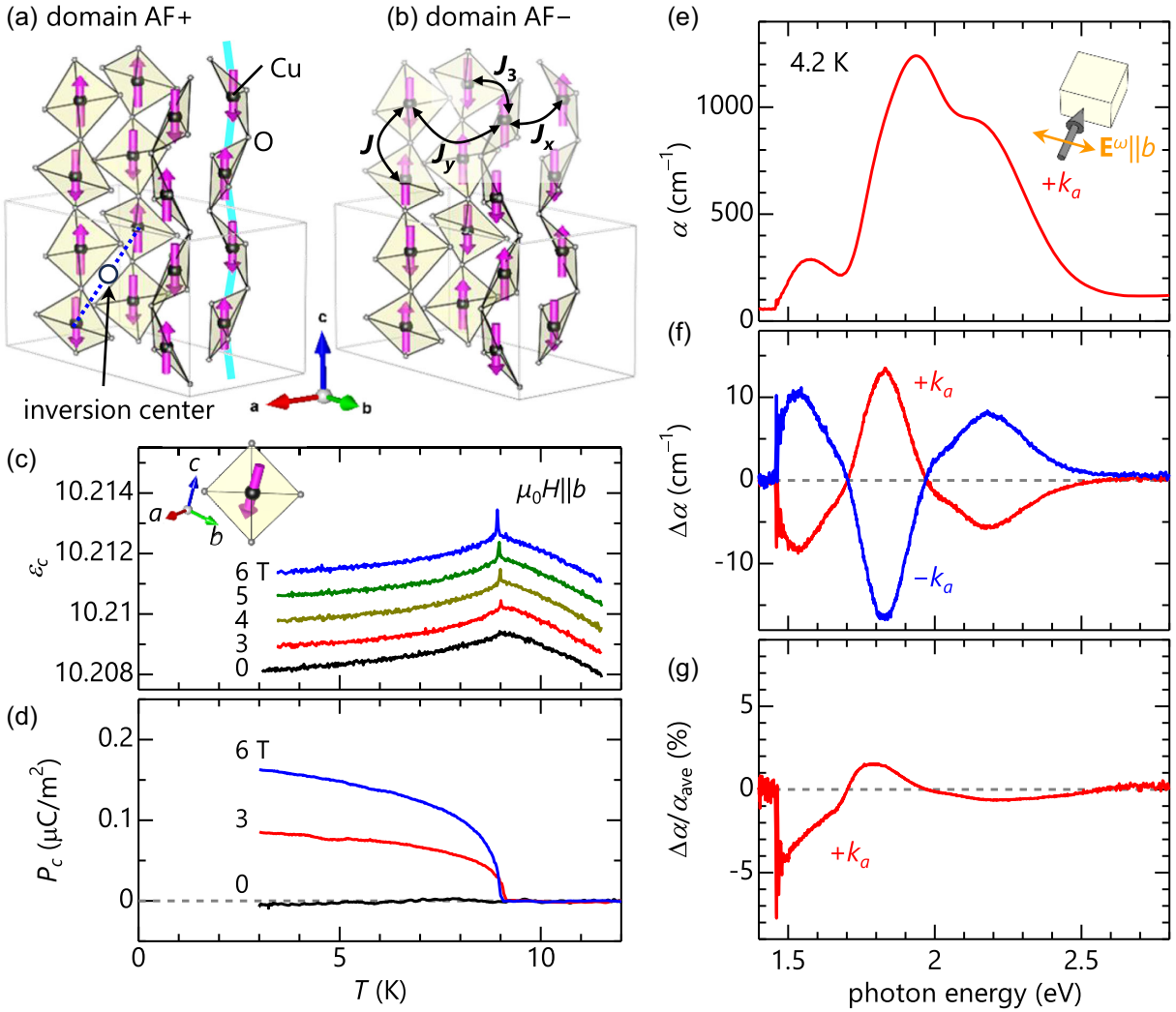

FIG. 2. (a),(b) Crystal and magnetic structures of $BaCu_2Si_2O_7$ for a pair of antiferromagnetic domains (a) AF+ and (b) AF−. Only Cu (black balls) and O atoms (small gray balls) are depicted for clarity. Magenta arrows indicate Cu^{2+} spins. The unit cell (gray box) contains eight distorted CuO_4 square units forming corner-sharing zigzag chains along the c axis. The white circle marks the inversion center. The intrachain interaction (J) and interchain chain interactions along a (J_x), b (J_y), and $\langle 110 \rangle$ directions (J_3) are shown in (b). (c),(d) Temperature dependence of (c) the dielectric constant and (d) the electric polarization along the c axis (ε_c and P_c, respectively) in an applied magnetic field along the b axis. For clarity, the ε_c data at 3, 4, 5, and 6 T are vertically shifted by +0.001, +0.002, +0.003, and +0.004, respectively. The inset of (c) shows the vertical view of the CuO_4 unit with the Cu^{2+} spin. (e)–(g) Spectra of (e) optical absorption coefficient α, (f) nonreciprocal directional dichroism (NDD) defined as $\Delta\alpha = \alpha(\mathrm{AF}+) - \alpha(\mathrm{AF}-)$, and (g) percentage difference of α [$\Delta\alpha/\alpha_{ave}$, where $\alpha_{ave} = \{\alpha(\mathrm{AF}+) - \alpha(\mathrm{AF}-)\}/2$]. The measurements were performed at 4.2 K without external fields after the ME cooling procedure (see text for details). The light propagation vector $\mathbf{k}$ is parallel to the $\pm a$ axis ($\pm k_a$) and the light polarization is parallel to the b axis ($\mathbf{E}^\omega \| b$). The inset of (e) shows an experimental geometry.

individually prepared by the so-called ME cooling procedure, more precisely by cooling the sample across T_N while applying $H_b E_c$ of opposite sign ($\mu_0 H_b = +0.1$ T and $E_c = \pm 190$ kV/m). The cooling fields were removed before each measurement. It is found that the $\Delta\alpha$ spectrum for $\mathbf{k}$ along the $+a$ axis ($+k_a$) measured at 5 K has a nonzero value, as shown by the red curve in Fig. 2(f). In addition, the $\Delta\alpha$ spectrum is completely reversed by reversing the direction of $\mathbf{k}$ [blue curve in Fig. 2(f)]. These results show that the finite $\Delta\alpha$ comes from the NDD. Furthermore, the percentage difference of α, $\Delta\alpha/\alpha_{ave}(\times 100)$, reaches up to 8% at about 1.45 eV, where $\alpha_{ave} = [\alpha(\mathrm{AF}+) + \alpha(\mathrm{AF}-)]/2$. The $\Delta\alpha$ signal decreases smoothly upon warming and its temperature dependence is scaled with that of the AF order parameter [33]. Also, the magnetic field (H_b) dependence of $\Delta\alpha$ at 5 K is approximately constant below the spin-flop transition field. These results indicate that the domain state remains unchanged and is robust to temperature and magnetic field. We also observe finite NDD signals for $\mathbf{E}^\omega \| c$, although the overall magnitude of $\Delta\alpha/\alpha_{ave}$ is found to

be smaller than that for $\mathbf{E}^{\omega}\|b$. The details are described in the Supplemental Material [39].

Here, we briefly discuss the possible mechanism of the NDD in $BaCu_2Si_2O_7$. In general, NDD in the visible to NIR range is explained by the interference between electric-dipole (E1) and magnetic-dipole (M1) transitions through the spin-orbit interaction, and the crystal field d-d transitions are dominant processes for $3d$ transition metal systems [23,25,26]. For Cu-based magnets composed of square planar CuO_4 units with weak local inversion breaking, very large NDD signals have been observed ($\Delta\alpha/\alpha_{\rm ave} \sim 100\%$ at $\sim$1.4 eV for CuB_2O_4 [25] and $\sim$40% at $\sim$1.6 eV for Bi_2CuO_4 [29]). They are attributed to the transition from a $d_{x^2-y^2}$ ground state (in the hole picture) to a d_{xy} first excited state hybridized with a d_{xz} (d_{yz}) state through the spin-orbit interaction due to the xy component of the Cu spin. Here, x, y, and z denote the local coordinate axes. Notably, for $BaCu_2Si_2O_7$ the geometry of the CuO_4 units is not far from the planar square geometry and the Cu spin (magnetic moment) has the xy component [see the inset of Fig. 2(c)]. Therefore, it is expected that the same transition process as in CuB_2O_4 and Bi_2CuO_4 is responsible for the NDD in $BaCu_2Si_2O_7$. This is the likely reason why the observed magnitude of $\Delta\alpha/\alpha_{\rm ave}$ (up to $\sim$8%) is comparable to those previously reported for other AFMs, despite the reduced ordered moments due to quantum fluctuations.

Utilizing the large NDD, we now visualize the AF domains in $BaCu_2Si_2O_7$. Figure 3(a) shows the optical microscopy image of a 35 μm thick sample at 5 K ($<T_{\rm N}$) after the zero-field cooling (ZFC), taken under conditions of $E_{\rm ph} = 1.9$ eV, k_a, and $\mathbf{E}^{\omega}\|b$. The image corresponds to the two-dimensional maps of α', which is defined as α at 5 K minus α in the paramagnetic phase (12.4 K) as a background. A clear two-level contrast is observed, indicating the coexistence of opposite AF domains in the bc plane. However, such a distribution of AF domains is absent along the thickness direction (a axis), otherwise a multilevel contrast would be observed. The DWs separating opposite AF domains run predominantly along the c axis, i.e., the direction of the spin chains. The width of individual domains is of the order of 0.1 mm along the b axis, while that along the c axis is more than 0.6 mm, i.e., a width of field of view along the c axis. Thus, the domain width along the c axis is about 10 or more times larger than that along the b axis. When the sample was heated above $T_{\rm N}$ and then cooled back with the ZFC condition, the domain pattern was changed, but the direction of the DWs was maintained, indicating the robustness of the DW anisotropy (see Supplementary Fig. S4). Figures 3(b) and 3(c) show the microscopic images after the ME cooling procedure with E_cH_b of opposite sign. It is found that a roughly monodomain state is achieved by the ME cooling, and the sign of E_cH_b determines the stabilized domain.

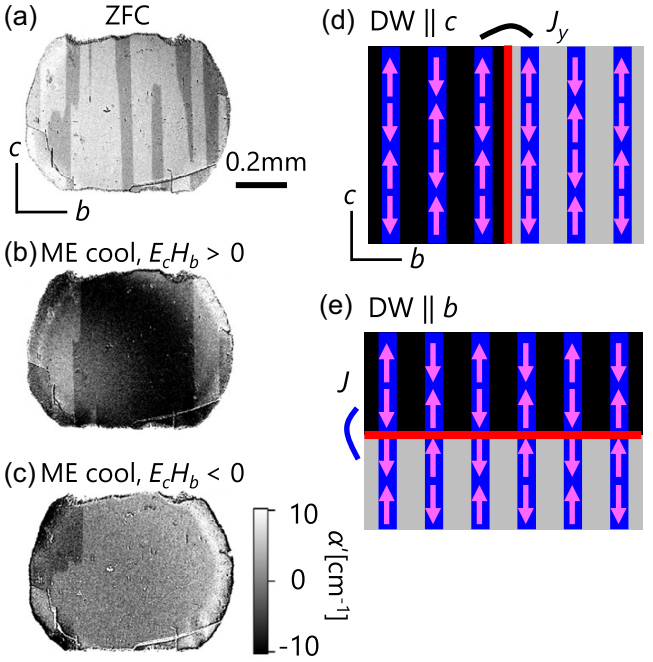

FIG. 3. Visualization of the antiferromagnetic domains in $BaCu_2Si_2O_7$. (a)–(c) Microscopy images of a sample after (a) zero-field cooling (ZFC), (b) ME cooling with $E_cH_b > 0$ ($E_c = +670$ kV/m and $\mu_0H_b = +0.2$ T), and (c) ME cooling with $E_cH_b < 0$ ($E_c = -670$ kV/m and $\mu_0H_b = +0.5$ T). The cooling fields were switched off before imaging. All the images were taken at 5 K under conditions of $E_{\rm ph} = 1.9$ eV, k_a, and $\mathbf{E}^{\omega}\|b$ in the absence of external fields. The images correspond to the two-dimensional map of α', which is the absorption coefficient α at 5 K minus α at 12.4 K. (d),(e) Schematics of a domain wall (DW) parallel to the (d) c axis and (e) b axis denoted by thick red lines. The magenta arrows represent the magnetic moments on the chains denoted by the blue lines. J_y in (d) and J in (e) indicate the interchain and intrachain interactions, respectively.

Furthermore, we investigate the isothermal control of AF domains with a strong electric field through the ME coupling. The following experiments were carried out on another sample with the narrower electrode spacing of 0.1 mm to increase the magnitude of the applied E_c. First, we cool the sample to 9.0 K just below $T_{\rm N}$ at zero field and then apply a bias magnetic field ($\mu_0H_b = 0.58$ T) to obtain a finite driving force (E_cH_b). In this initial state, the DWs are again parallel to the c axis [Fig. 4(a)]. We then visualize the evolution of the domains under the application of $E_c = 0 \rightarrow +4$ [Fig. 4(b)] $\rightarrow -4$ MV/m [Fig. 4(c)]. As highlighted by the dotted lines, the DWs are slightly shifted so that the bright region is increased (decreased) by applying $E_c = +4$ MV/m (-4 MV/m). Such a DW shift was observed only at temperatures close to $T_{\rm N}$, and the domain pattern is robust at lower temperatures. It is noteworthy that the direction of the DWs is maintained during the movement. These results indicate that the DW anisotropy also

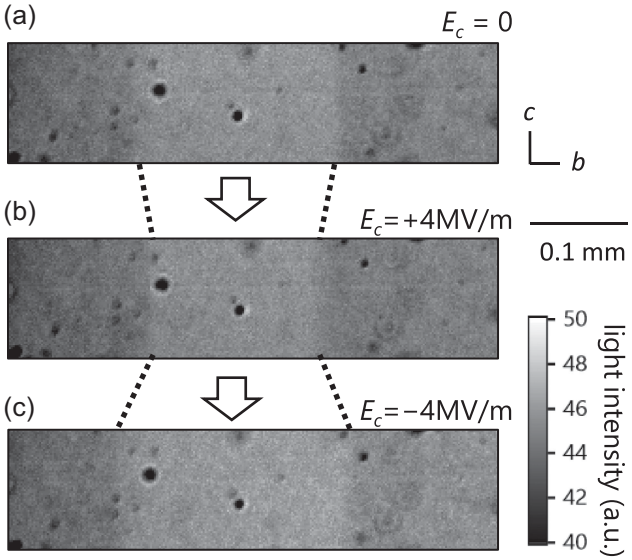

FIG. 4. Visualization of electric-field-driven displacement of antiferromagnetic domain walls. (a)–(c) Transmission microscopy images of a sample at 9.15 K (a) before the application of an electric field along the c axis (E_c), (b) after the application of $E_c = +4$ MV/m, and (c) after the subsequent application of $E_c = -4$ MV/m. During the experiments, the 0.58 T magnetic field was always applied along the b axis. Dotted lines indicate the displacement of antiferromagnetic domain walls.

governs their motion driven by the application of the electric field.

Finally, we discuss the origin of the observed DW anisotropy. Figures 3(d) and 3(e) show schematic spin arrangements near the DW$\|c$ and the DW$\|b$, respectively. The creation of the DW$\|b$ costs the energy governed by $J = 24.1$ meV, which is 2 orders of magnitude larger than $J_y = 0.20$ meV for the DW$\|c$ (Ref. [33]). This suggests that the DW$\|c$ is preferable than the DW$\|b$, which is consistent with the present observation. In this scenario, the ratio of the domain wall lengths along the c (L_c) and b (L_b) axes should be $L_c/L_b \sim J/J_y \sim 100$. However, this value is far from the experimental values of $L_c/L_b \sim 10$, which are obtained from two different domain patterns (see Sec. 6 of Supplemental Material). Therefore, another factor should also be considered to understand the DW formation. The sample size in the bc plane is less anisotropic (about 1 and 2 mm along the c and b axes, respectively) and thus does not appear to be related to the DW anisotropy. The DW represents a LRO destruction and can therefore be associated with spin excitations that result from the LRO destruction, too. It is interesting to examine whether magnons and/or spinons are involved in the formation of the DWs in $BaCu_2Si_2O_7$. To our knowledge, there is no relevant theory available. Future work is needed to understand the microscopic origin of the DW anisotropy in the q1D-QAFM. We note that $Cs_2Cu_2Mo_3O_{12}$ is another candidate for q1D-QAFMs with broken space-inversion and time-reversal symmetries in the absence of external fields since H-induced P and an AF order with a magnetic propagation vector (0, 0, 0) have recently been reported [41]. The present domain imaging technique could be applied to this material, and if so, the comparison of AF domains between $Cs_2Cu_2Mo_3O_{12}$ and $BaCu_2Si_2O_7$ is of interest.

In conclusion, we successfully visualize the spatial distribution of antiferromagnetic domains in the quasi-one-dimensional $S = 1/2$ quantum antiferromagnet, $BaCu_2Si_2O_7$, by exploiting the nonreciprocal directional dichroism allowed by the breaking of space-inversion and time-reversal symmetries. We find that the domain pattern is anisotropic, and the domain walls are predominantly parallel to the c axis, i.e., the direction of the spin chains. This domain wall orientation is maintained even during the electric-field-induced motion of the antiferromagnetic domains. These observations are roughly explained by the quasi-one-dimensional nature of the exchange interactions. The situation is in stark contrast to the complex domain patterns and domain walls in quasi-two-dimensional and three-dimensional antiferromagnets, whose formation mechanism cannot be easily understood [28,29,42,43]. The present study therefore raises an interesting future question as to whether the domain pattern observed in $BaCu_2Si_2O_7$ is a material-specific property or intrinsic to quasi-one-dimensional quantum magnets.

Acknowledgments—K. K. acknowledges support from JSPS KAKENHI Grant No. JP19H01847 and No. JP24K00575, the MEXT Leading Initiative for Excellent Young Researchers (LEADER), the Murata Science Foundation, and the Iketani Science and Technology Foundation. T. K. acknowledges support from JSPS KAKENHI Grants No. JP19H05823, No. JP21H04436, and No. JP21H04988.

[1] H. J. Mikeska and Z. K. Kolezhuk, *One-Dimensional Magnetism* (Springer, Berlin, 2004), Vol. 645.
[2] A. Vasiliev, O. Volkova, E. Zvereva, and M. Markina, npj Quantum Mater. **3**, 18 (2018).
[3] S. E. Dutton, M. Kumar, M. Mourigal, Z. G. Soos, J.-J. Wen, C. L. Broholm, N. H. Andersen, Q. Huang, M. Zbiri, R. Toft-Petersen, and R. J. Cava, Phys. Rev. Lett. **108**, 187206 (2012).
[4] F. D. M. Haldane, Phys. Lett. **93A**, 464 (1983).
[5] M. Yamashita, T. Ishii, and H. Matsuzaka, Coord. Chem. Rev. **198**, 347 (2000).
[6] N. Büttgen, K. Nawa, T. Fujita, M. Hagiwara, P. Kuhns, A. Prokofiev, A. P. Reyes, L. E. Svistov, K. Yoshimura, and M. Takigawa, Phys. Rev. B **90**, 134401 (2014).
[7] N. Motoyama, H. Eisaki, and S. Uchida, Phys. Rev. Lett. **76**, 3212 (1996).
[8] K. M. Kojima, Y. Fudamoto, M. Larkin, G. M. Luke, J. Merrin, B. Nachumi, Y. J. Uemura, N. Motoyama, H. Eisaki, S. Uchida, K. Yamada, Y. Endoh, S. Hosoya,

B. J. Sternlieb, and G. Shirane, Phys. Rev. Lett. **78**, 1787 (1997).
[9] A. Zheludev, M. Kenzelmann, S. Raymond, E. Ressouche, T. Masuda, K. Kakurai, S. Maslov, I. Tsukada, K. Uchinokura, and A. Wildes, Phys. Rev. Lett. **85**, 4799 (2000).
[10] I. Tsukada, Y. Sasago, K. Uchinokura, A. Zheludev, S. Maslov, G. Shirane, K. Kakurai, and E. Ressouche, Phys. Rev. B **60**, 6601 (1999).
[11] T. Lancaster, S. J. Blundell, M. L. Brooks, P. J. Baker, F. L. Pratt, J. L. Manson, C. P. Landee, and C. Baines, Phys. Rev. B **73**, 020410(R) (2006).
[12] B. Lake, A. M. Tsvelik, S. Notbohm, D. Alan Tennant, T. G. Perring, M. Reehuis, C. Sekar, G. Krabbes, and B. Büchner, Nat. Phys. **6**, 50 (2010).
[13] Z. Wang, M. Schmidt, A. K. Bera, A. T. M. N. Islam, B. Lake, A. Loidl, and J. Deisenhofer, Phys. Rev. B **91**, 140404(R) (2015).
[14] E. G. Sergeicheva, S. S. Sosin, L. A. Prozorova, G. D. Gu, and I. A. Zaliznyak, Phys. Rev. B **95**, 020411(R) (2017).
[15] N. Hedrich, K. Wagner, O. V. Pylypovskyi, B. J. Shields, T. Kosub, D. D. Sheka, D. Makarov, and P. Maletinsky, Nat. Phys. **17**, 574 (2021).
[16] Z. Ni, A. V. Haglund, H. Wang, B. Xu, C. Bernhard, D. G. Mandrus, X. Qian, E. J. Mele, C. L. Kane, and L. Wu, Nat. Nanotechnol. **16**, 782 (2021).
[17] J. Takeya, I. Tsukada, Y. Ando, T. Masuda, K. Uchinokura, I. Tanaka, R. S. Feigelson, and A. Kapitulnik, Phys. Rev. B **63**, 214407 (2001).
[18] O. Breunig, M. Garst, A. Rosch, E. Sela, B. Buldmann, P. Becker, L. Bohatý, R. Müller, and T. Lorenz, Phys. Rev. B **91**, 024423 (2015).
[19] M. Gillig, X. Hong, P. Sakrikar, G. Bastien, A. U. B. Wolter, L. Heinze, S. Nishimoto, B. Büchner, and C. Hess, Phys. Rev. B **104**, 235129 (2021).
[20] J. Baruchel, M. Schlenker, and B. Barbara, J. Magn. Magn. Mater. **15–18**, 1510 (1980).
[21] Y. Geng, H. Das, A. L. Wysocki, X. Wang, S.-W. Cheong, M. Mostovoy, C. J. Fennie, and W. Wu, Nat. Mater. **13**, 163 (2014).
[22] M. Fiebig, D. Fröhlich, G. Sluyterman V. L., and R. V. Pisarev, Appl. Phys. Lett. **66**, 2906 (1995).
[23] L. D. Barron and J. Vrbancich, Mol. Phys. **51**, 715 (1984).
[24] G. L. J. A. Rikken and E. Raupach, Nature (London) **390**, 493 (1997).
[25] M. Saito, K. Taniguchi, and T. Arima, J. Phys. Soc. Jpn. **77**, 013705 (2008).
[26] T. Arima, J. Phys. Condens. Matter **20**, 434211 (2008).
[27] I. Kézsmárki, N. Kida, H. Murakawa, S. Bordács, Y. Onose, and Y. Tokura, Phys. Rev. Lett. **106**, 057403 (2011).
[28] K. Kimura, T. Katsuyoshi, Y. Sawada, S. Kimura, and T. Kimura, Commun. Mater. **1**, 39 (2020).
[29] K. Kimura, Y. Otake, and T. Kimura, Nat. Commun. **13**, 697 (2022).
[30] T. Sato, N. Abe, Y. Tokunaga, and T. H. Arima, Phys. Rev. B **105**, 094417 (2022).
[31] K. Kimura and T. Kimura, APL Mater. **11**, 100902 (2023).
[32] M. Fiebig, J. Phys. D **38**, R123 (2005).
[33] M. Kenzelmann, A. Zheludev, S. Raymond, E. Ressouche, T. Masuda, P. Böni, K. Kakurai, I. Tsukada, K. Uchinokura, and R. Coldea, Phys. Rev. B **64**, 054422 (2001).
[34] S. Hayami, H. Kusunose, and Y. Motome, J. Phys. Condens. Matter **28**, 395601 (2016).
[35] S. Kimura, K. Kakihata, Y. Sawada, K. Watanabe, M. Matsumoto, M. Hagiwara, and H. Tanaka, Nat. Commun. **7**, 12822 (2016).
[36] F. Schrettle, S. Krohns, P. Lunkenheimer, A. Loidl, E. Wulf, T. Yankova, and A. Zheludev, Phys. Rev. B **87**, 121105(R) (2013).
[37] Y. Naito, K. Sato, Y. Yasui, Y. Kobayashi, Y. Kobayashi, and M. Sato, J. Phys. Soc. Jpn. **76**, 023708 (2007).
[38] V. N. Glazkov, G. Dhalenne, A. Revcolevschi, and A. Zheludev, J. Phys. Condens. Matter **23**, 086003 (2011).
[39] See Supplemental Material at http://link.aps.org/supplemental/10.1103/PhysRevLett.133.086701 for experimental details and additional experimental data (n.d.).
[40] K. Momma and F. Izumi, J. Appl. Crystallogr. **44**, 1272 (2011).
[41] D. Flavián, P. A. Volkov, S. Hayashida, K. Yu. Povarov, S. Gvasaliya, P. Chandra, and A. Zheludev, Phys. Rev. Lett. **130**, 216501 (2023).
[42] B. B. Van Aken, J. P. Rivera, H. Schmid, and M. Fiebig, Phys. Rev. Lett. **101**, 157202 (2008).
[43] M. S. Wörnle, P. Welter, M. Giraldo, T. Lottermoser, M. Fiebig, P. Gambardella, and C. L. Degen, Phys. Rev. B **103**, 094426 (2021).